PHILOSOPHICAL MAGAZINE A, 2001, VOL. 81, NO. 2, 467–478

On the existence of superlattice intrinsic stacking fault–superlattice extrinsic stacking fault coupled pairs in an $L1_2$ alloy

G. F. DIRRAS† and J. DOUIN‡

Laboratoire d'Etude des Microstructures, Unite Mixte de Recherche associée au CNRS–ONERA 104, 29 avenue de La Division Leclerc, BP 72, 92322 Châtillon, France

[*Received 20 March 2000 and accepted in revised form 15 May 2000*]

ABSTRACT

Double-faulted ribbons of stacking faults on the same {111} plane have been found in a $L1_2$ pseudobinary Ni_3Ge-Fe_3Ge compound. They stem from the interaction of coplanar ⟨110⟩ superdislocations giving rise to ⟨112⟩ dislocations, which subsequently dissociate into three identical $\frac{1}{3}\langle 112\rangle$ Shockley partials. It is shown that, provided that a larger core relaxation of the $\frac{1}{3}\langle 112\rangle$ partial dislocations is assumed, the threefold dissociated configuration has a lower energy than the antiphase-boundary dissociated configuration.

§1. INTRODUCTION

It is well known that the dissociation mode strongly influences the behaviour of dislocations as it may constrain dislocations to glide in specific planes, affecting cross-slip as well. The dissociation mode itself is very dependent on the energy of the fault(s) created during the dissociation. For example, twinning is favoured in materials where the formation of stacking faults is easy. Also, the flow stress peak observed in numerous $L1_2$ alloys is attributed to the formation of Kear–Wilsdorf locks, directly resulting from the dissociation of ⟨110⟩ superdislocations according to

$$\langle 110\rangle \rightarrow \tfrac{1}{2}\langle 110\rangle + \mathrm{APB} + \tfrac{1}{2}\langle 110\rangle, \tag{1}$$

where APB denotes an antiphase boundary. The dissociation (1), in turn, relies on the relative energies of the APB on the {001} and {111} planes (Kear and Wilsdorf 1962). This type of dissociation is the most frequently encountered in $L1_2$ alloys but other dissociation processes exist. For example, in some $L1_2$ alloys at low temperatures the negative temperature dependence of the flow stress in octahedral slip was claimed to originate from the dissociation under the superlattice stacking faults coupled dissociation (Tichy *et al.* 1986a,b) according to

$$\langle 110\rangle \rightarrow \tfrac{1}{3}\langle 121\rangle + \mathrm{SISF} + \tfrac{1}{3}\langle 21\bar{1}\rangle \tag{2}$$

† Email: dirras@onera.fr.
‡ Email: douin@onera.fr.

Philosophical Magazine A ISSN 0141–8610 print/ISSN 1460-6992 online
http://www.tandf.co.uk/journals

where SISF indicates a superlattice intrinsic stacking fault. In fact, in $L1_2$ alloys, observation of SISFs is a common feature, for example, in Ni_3Ga (Takeuchi and Kuramoto 1973), in Ni_3Al-based alloy (Kear *et al.* 1970, Oblak and Kear 1971) and Zr_3Al (Howe *et al.* 1974). Except in Zr_3Al, where edge dislocations dissociate to form a SISF ribbon (Douin 1991), these stacking faults are usually related to debris resulting from dislocation interactions (Veyssière and Douin 1994).

Meanwhile, superlattice extrinsic stacking faults (SESFs) are only rarely encountered in $L1_2$ alloys as the energy of extrinsic faults is supposed to exceed the intrinsic fault energy. Contrary to $L1_2$, in TiAl with the parent structure $L1_0$, SESF dipoles are present in a high density (Hug *et al.* 1986). In this case, SESF dipoles result from the decomposition and dissociation of [101] dislocations according to

$$[101] \rightarrow \tfrac{1}{2}[1\bar{1}0] + \text{APB} + \tfrac{1}{3}[112] + \text{SESF} + \tfrac{1}{6}[112]. \tag{3}$$

The observation of extrinsic stacking faults (ESFs) has been reported in numerous fcc alloys and pure silver in extended nodes of dislocations (for example Loretto (1965)).

In the Ag–12.5 at.% In alloy, parallel arrays of intrinsic stacking faults (ISFs)–ESFs have been observed (Gallagher 1966) resulting from the dissociation by glide of $\frac{1}{2}\langle 112\rangle$ dislocations, according to

$$\tfrac{1}{2}\langle 112\rangle \rightarrow \tfrac{1}{6}\langle 112\rangle + \text{ISF} + \tfrac{1}{6}\langle 112\rangle + \text{ESF} + \tfrac{1}{6}\langle 112\rangle. \tag{4}$$

Threefold dissociation leading to an ISF–ESF pair has also been observed in $L1_0$ alloys (Ivchenko *et al.* 1986, Hug 1988) as well as in $D0_{22}$ alloys (Vanderschaeve 1984, François 1992) but, in these structures, $\frac{1}{2}\langle 112]$ dislocations are not uncommon since $\frac{1}{2}\langle 112]$ is a perfect translation of the crystal (third-shortest perfect translation in the $D0_{22}$ structure). Contrary to the $L1_0$ and $D0_{22}$ structures, in the $L1_2$ structure, $\frac{1}{2}\langle 112\rangle$ is not a perfect translation vector of the lattice. Moreover, dislocations with a $\langle 112\rangle$ Burgers vector should spontaneously decompose according to

$$\langle 112\rangle \rightarrow \langle 101\rangle + \langle 011\rangle, \tag{5}$$

since self-energy, or more simply the b^2 or Frank criterion would favour the right-hand side of reaction (5). To the present authors' knowledge, $\langle 112\rangle$ dislocations in a $L1_2$ alloy have only been reported once, in manganese-stabilized Al_3Ti, and their formation was claimed to result from $\langle 110\rangle$ dislocations interactions (Douin *et al.* 1995).

The decomposition process of a $\langle 112\rangle$ dislocation could be in some cases replaced by dissociation provided that the energy of the entire configuration is lowered. It is the aim of this paper to report the observation in a $L1_2$ alloy of $\langle 112\rangle$ dislocations resulting from the interaction of different $\langle 101\rangle$ dislocations and their dissociation to form a coupled ISF–ESF ribbon, and to discuss the stability of such three-fold dissociated dislocations.

§2. Experimental details

A pseudobinary $L1_2$ compound of $(Ni_xFe_{1-x})_3Ge$ type containing 55 at.% Ni and 20 at.% Fe was prepared on the basis of the procedure given by Suzuki *et al.* (1980). It was strained at 823 K under uniaxial compression to about 2% of permanent strain and at a nominal strain rate of 10^{-4} s^{-1}. The deformation temperature is above the peak stress anomaly temperature that occurs at about 673 K for this composition of the alloy. Following compressive experiments, the deformed speci-

mens were sliced at 45° to the compression axis. Discs of about 3 mm diameter and 400 μm thick were thus produced and subsequently ground to a thickness of 150–200 μm. Finally, the discs were electropolished in a mixture of 95% butoxyl 2-ethanol and 5% perchioric acid at −35°C in a Struers Tenupol III apparatus. The thin foils were examined using a JEOL 200 CX electron microscope operating at 200 kV under weak-beam conditions. The weak-beam conditions have been ensured by choosing imaging conditions leading to a value of the deviation parameter s_g of the order of or greater than $0.15\,nm^{-1}$, that is at least **g**–4**g** for **g** = 220, **g**–5**g** for **g** = 111 and **g**–6**g** for **g** = 200 (Douin *et al*. 1998).

§ 3. Results

The overall dislocation morphology and distribution of dislocations after deformation at 823 K is shown in figure 1 and at a higher magnification in figure 2. The microstructure consists mainly of two families of ⟨110⟩-type superdislocations, dissociated into two identical superpartials bounding an antiphase boundary, as described by equation (1) and usually found in most $L1_2$ alloys. Contrast experiments have shown that they have respectively [110] (horizontally inclined superdislocations, labelled I in figure 2) and $[\bar{1}10]$ (vertical superdislocations, labelled II) Burgers vectors. Note the frequent fluctuations of the dissociation width that occurs along superdislocations II when they interact with dislocations I (points 1 and 2 in figure 2). Stereographic analyses have shown that both dislocations I and dislocations II are mostly screw dislocations. Some superdislocation dipoles, denoted SD, were also found.

The most interesting feature on which we shall focus in the following is the observation of stacking faults (white arrows in figures 1 and 2). Close observation shows that the faulted defect exhibits in fact two linked faulted ribbons of unequal widths bounded by three superpartials. Thus, they do not result from dissociation according to equation (2), nor are they superlattice stacking-fault dipoles resulting from pinning of one superpartial during movement. They also do not appear to be faulted loops bordered by a $\frac{1}{3}\langle 112\rangle$ dislocation, as found in many $L1_2$ alloys as a by-product of the deformation.

The faults often extend over a large distance and usually end at the surface of the foil (see for example the fault in the centre of figure 1). When they end within the foil, the termination is always associated with the presence of ⟨110⟩ dislocations. Figure 3 shows a series of micrographs obtained under different weak-beam imaging conditions of one such double ribbon of stacking faults, which starts and ends within the foil. From this observation, it is clear that the configuration results from the interaction of two ⟨110⟩ dislocations (denoted I and II in figure 3) with a $[\bar{1}10]$ and a [011] Burgers vector respectively, both dissociated, lying and gliding in the $(11\bar{1})$ plane. It should be noted that $[\bar{1}10]$ curvilinear superdislocations are present in the sample with a high density, as well as [110] superdislocations (see figure 1), while [011] mixed superdislocations are seen with a lower density. In fact, the [011] dislocations are almost always observed in relation with the formation of double ribbons of stacking faults. It is thus assumed that a local interaction of superdislocations lying in the same glide plane is a prerequisite for the faulted configuration to occur.

Two possibilities exist for the interaction of $[\bar{1}10]$ and [011] superdislocations:

$$[1\bar{1}0] + [011] \rightarrow [101] \tag{6}$$

or

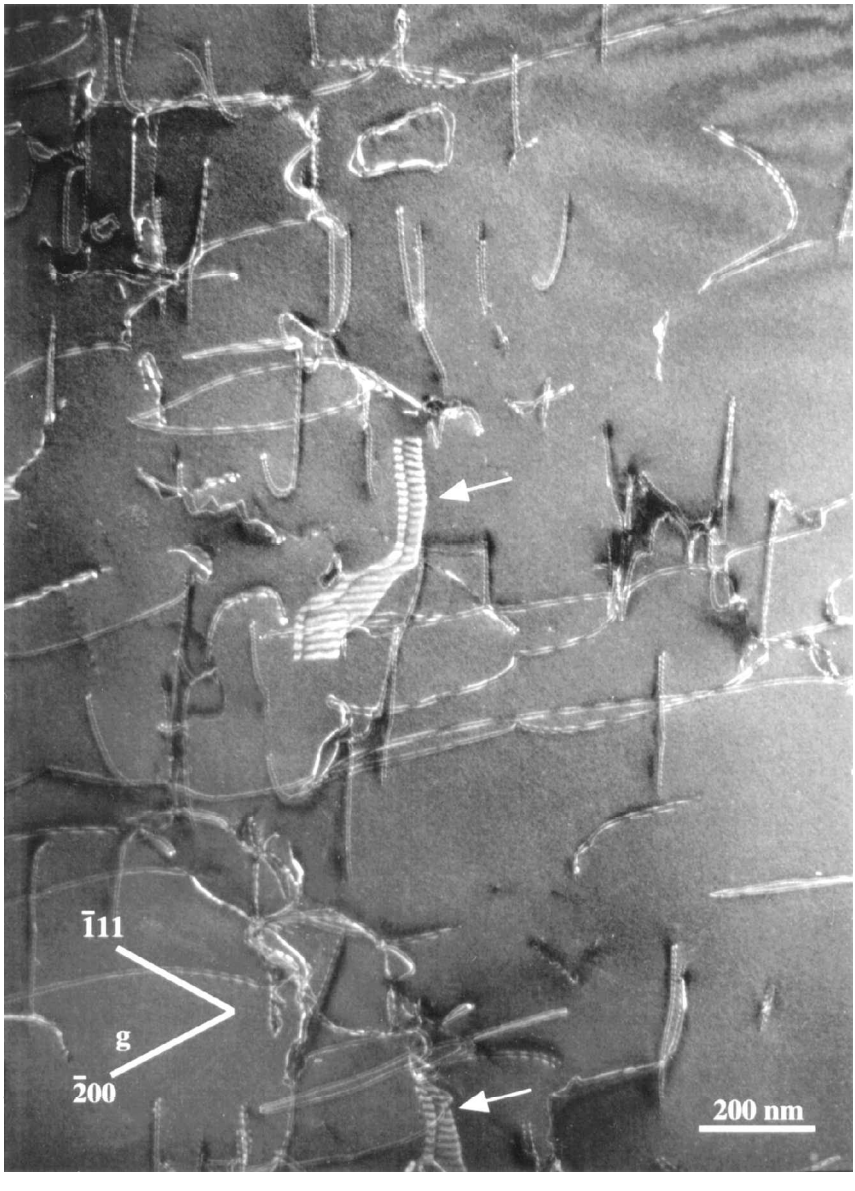

Figure 1. Weak-beam transmission electron micrograph of dislocations found in $Ni_{0.55}Fe_{0.2}Ge_{0.2}$ deformed in compression at 823 K (dark-field weak-beam image with the $\mathbf{g} = \bar{2}00$ reflection; downwards direction of electrons, $\mathbf{B} = [01\bar{1}]$). Horizontal dislocations have a [110] Burgers vector and vertical dislocations have a $[\bar{1}10]$ Burgers vector. Faulted configurations are indicated by white arrows.

$$[\bar{1}10] + [011] \rightarrow [\bar{1}21] \tag{7}$$

and their equivalent opposites, both interaction products being contained in the $(11\bar{1})$ plane. Figure 3 shows that the two stacking-fault vectors are collinear as they always present the same visibility–invisibility conditions whatever the reflection **g** used. The conditions of visibility of the three partial dislocations along the faults

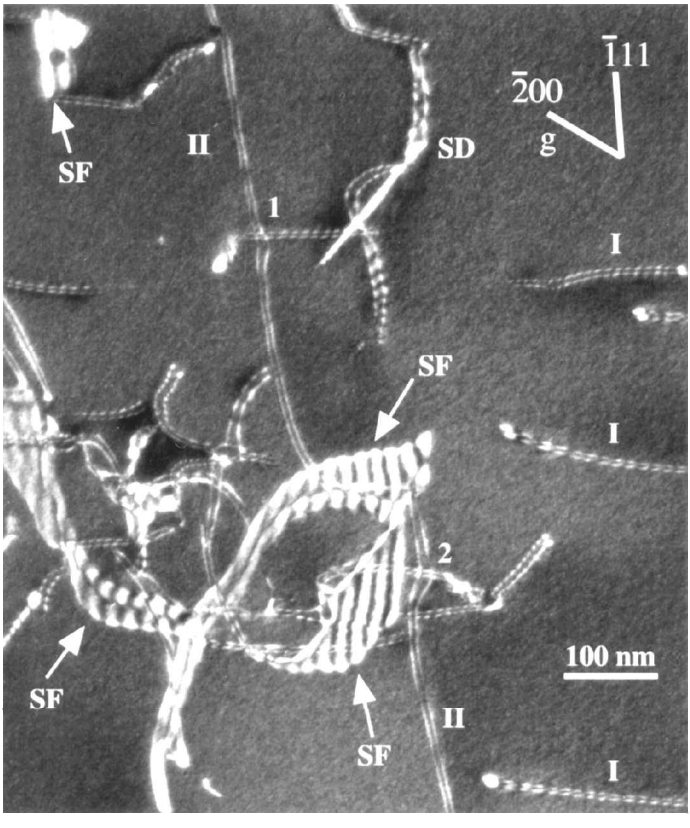

Figure 2. Another example of the deformation microstructure in $Ni_{0.55}Fe_{0.2}Ge_{0.2}$ ($\mathbf{g} = \bar{2}00$; $\mathbf{B} = [01\bar{1}]$). Dislocations I and II have [011] and [110] Burgers vectors respectively. Note the fluctuation of the dissociation width that occurs along super-dislocations II when they interact with dislocations I (points 1 and 2 in figure 2). SF denotes stacking fault, and SD super-dipole.

are not obvious since the fringes of the faults may overlap their images. However, it is sufficient to remark that the Burgers vector of a partial dislocation bordering only one fault is equal (modulus of a perfect translation of the lattice) to the fault vector **R**. Thus, since the fringes are in contrast when $\mathbf{g}\cdot\mathbf{R}$ is not zero or not integer (for example Edington (1975)), the dislocation can be considered as in contrast when the fault is visible. Note that the reverse is not true since, when $\mathbf{g}\cdot\mathbf{R}$ is integer, the fault is out of contrast while the bordering partial remains visible. It follows that the three partial dislocations have collinear Burgers vectors since they always present the same visibility conditions; they are in contrast for $\mathbf{g} = \bar{2}00$, $\bar{1}\bar{1}\bar{1}$, $0\bar{2}0$, $2\bar{2}0$ and $0\bar{2}\bar{2}$ (figures 3 (*a*), (*b*), (*c*), (*d*) and (*f*) respectively) and out of contrast for $\mathbf{g} = 202$ (figure 3 (*e*)). This is consistent only with a Burgers vector parallel to $[\bar{1}21]$, showing that reaction (7) has occurred, but followed by a subsequent dissociation of the $\langle 112\rangle$ dislocation, according to

$$[\bar{1}21] \rightarrow \tfrac{1}{3}[\bar{1}21] + \text{SISF} + \tfrac{1}{3}[\bar{1}21] + \text{SESF} + \tfrac{1}{3}[\bar{1}21]. \tag{8}$$

The vectors associated with the faults are $\frac{1}{3}[\bar{1}21]$ and $\frac{2}{3}[\bar{1}21]$ (or equivalently $-\frac{1}{3}[\bar{1}21]$) respectively. This explains why the fringes resulting from the contrast of the stacking

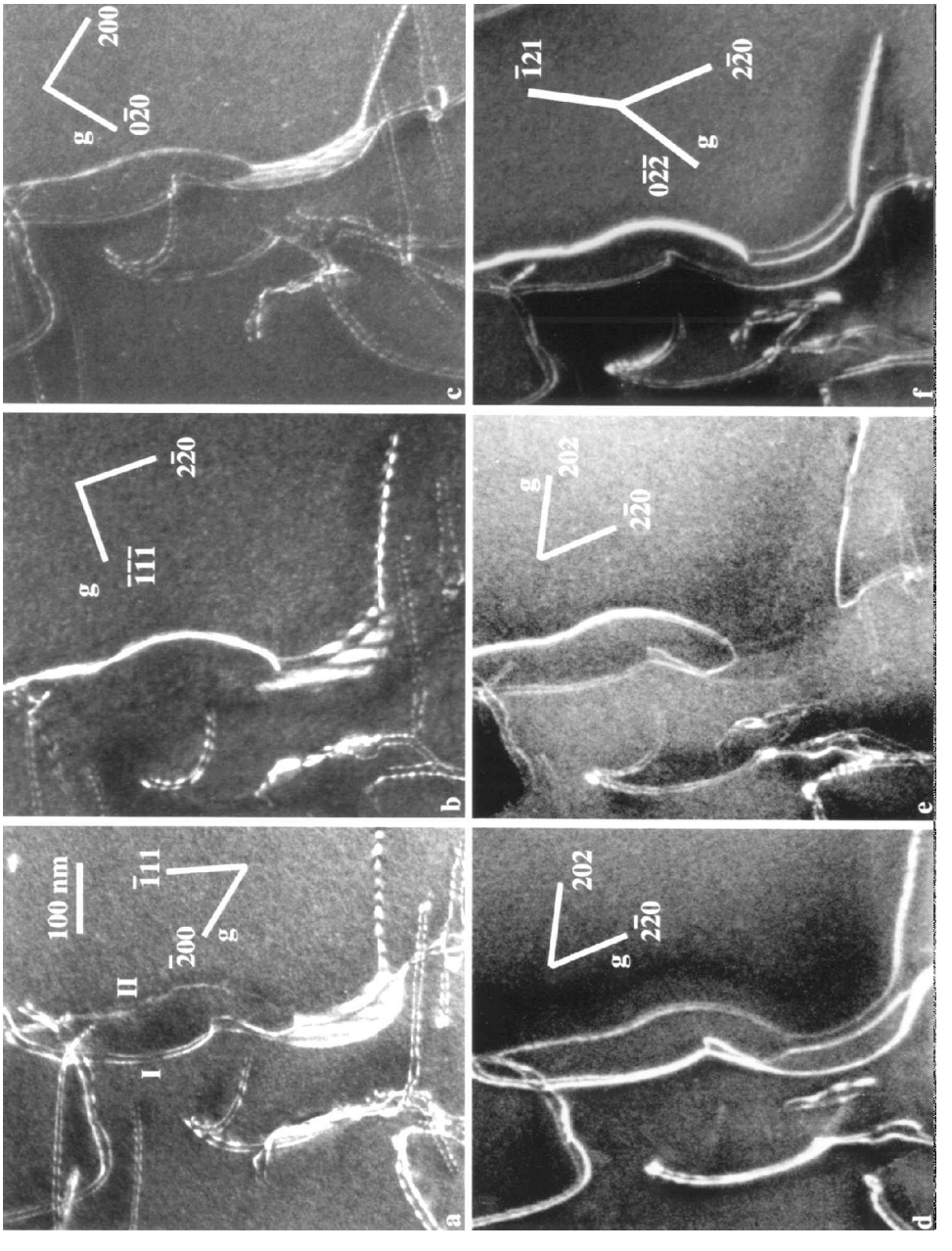
100 nm
I
II
$\bar{2}00$
$\bar{1}11$
g
a
g
$\bar{1}\bar{1}\bar{1}$
$2\bar{2}0$
b
g
200
$0\bar{2}0$
c
g
202
$2\bar{2}0$
e
202
g
$2\bar{2}0$
d
$\bar{1}21$
$0\bar{2}\bar{2}$
g
$2\bar{2}0$
f

faults, when visible, are shifted regarding to each other as the phase shifts ($2\pi\mathbf{g}\cdot\mathbf{R}$) of the SISF and the SESF are never equal. It can also be verified that the faulted ribbons are out of contrast when viewed in the $(11\bar{1})$ plane, whatever the 220-type diffraction vector on this plane (see figures 3 (*d*), (*e*) and (*f*)). This confirms that the fault vectors and thus the complete configuration are contained in the $(11\bar{1})$ plane.

Reaction (8) also implies the formation of the small segments a, b, c and d in figure 4 with a $\frac{1}{3}\langle 112\rangle$-type Burgers vector and geometrically necessary closure segments with $\frac{1}{6}\langle 11\bar{2}\rangle$-type Burgers vectors. The latter are hardly visible because they are too small while, in the present weak-beam conditions, the former show either a low contrast when $\mathbf{g}\cdot\mathbf{b} = \pm 2/3$ (figures 3 (*b*) and (*c*) for segments a and c; figures 3 (*a*) and (*c*) for segments b and d) or a stronger contrast when $\mathbf{g}\cdot\mathbf{b} = \pm 4/3$ (figures 3 (*a*) for segments a and c; figure 3 (*b*) for segments b and d). Note also that segments b and d are out of contrast for $\mathbf{g} = 2\bar{2}0$ (figure 3 (*d*)) while segments a and c are out of contrast for $g = 0\bar{2}\bar{2}$ (figure 3 (*f*)), allowing complete determination of the dislocations involved (figure 4).

§4. Discussion

4.1. *Stacking-fault energies*

The stability of the overall configuration resulting from reaction (8) obviously depends on the energies of the two stacking faults. We shall consider infinite and parallel dislocations assuming at first that the bordering $\frac{1}{3}\langle 112\rangle$ and $\frac{1}{6}\langle 112\rangle$ partial dislocations do not play a significant role. Assuming linear elasticity, the interaction energies by unit length between the three identical infinite partials located in the same plane, for a given line direction, are

$$\begin{aligned} E_{12} &= K \ln\left(\frac{d_i}{R}\right), \\ E_{23} &= K \ln\left(\frac{d_e}{R}\right), \\ E_{13} &= K \ln\left(\frac{d_i + d_e}{R}\right), \end{aligned} \tag{9}$$

where d_i and d_e are the widths of the intrinsic and extrinsic faults respectively. As the partial dislocations are identical and parallel, the same K pre-factor is effective. The total energy of the threefold configuration is then

Figure 3. Contrast experiments of a double ribbon of stacking faults created by the interaction of two $\langle 110\rangle$ dislocations. (*a*) $\mathbf{g} = \bar{2}00$; $\mathbf{B} = [01\bar{1}]$; dislocation II is out of contrast, except for the residual contrast of its bottom part which results from the strong edge character of the line **u** and thus the high value of $\mathbf{g}\cdot\mathbf{b}\otimes\mathbf{u}$ (Edington 1975, p. 11). (*b*) $\mathbf{g} = \bar{1}\bar{1}\bar{1}$; $\mathbf{B} = [11\bar{2}]$; dislocation I is out of contrast. (*c*) $\mathbf{g} = 0\bar{2}0$; $\mathbf{B} = [00\bar{1}]$; all the involved features, superdislocations and faulted double ribbons, are visible. (*d*) $\mathbf{g} = 2\bar{2}0$; $\mathbf{B} = [\bar{1}\bar{1}1]$; the two ribbons and segments **b** and **d** are out of contrast (for segment labelling see the sketch in figure 4). (*e*) $\mathbf{g} = 202$; $\mathbf{B} = [\bar{1}\bar{1}1]$; the faulted ribbons and the three partials are out of contrast, while the $\langle 110\rangle$ superdislocations and the four segments **a**, **b**, **c** and **d** are still in contrast. (*f*) $\mathbf{g} = 0\bar{2}\bar{2}$; $\mathbf{B} = [\bar{1}\bar{1}1]$; the two ribbons and the segments **a** and **c** are out of contrast; the screw $[\bar{1}21]$ direction is indicated.

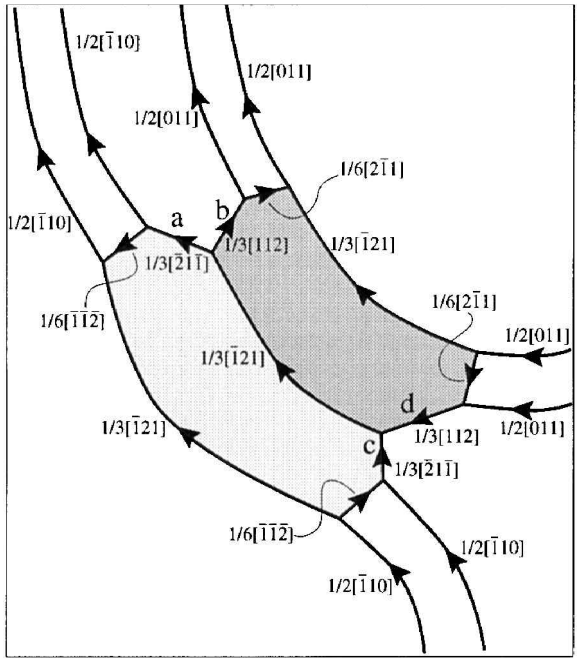

Figure 4. Schematic diagram of the configuration presented in figure 3. The Burgers vectors of the partial dislocations are indicated.

$$E_T = 3E_{self} + K \ln\left(\frac{d_i d_e (d_i + d_e)}{R^3}\right) + \gamma_i d_i + \gamma_e d_e, \tag{10}$$

where E_{self} is the self-energy of a partial dislocation in the given orientation, and γ_i and γ_e are the energies of the intrinsic and extrinsic faults respectively.

At equilibrium,

$$\begin{aligned} \frac{\partial E_T}{\partial d_i} &= 0, \\ \frac{\partial E_T}{\partial d_e} &= 0, \end{aligned} \tag{11}$$

which leads to

$$\frac{\gamma_i}{\gamma_e} = \frac{2 + d_e/d_i}{2 + d_i/d_e} \ . \tag{12}$$

Note that equation (12) is valid for any three identical partials in the same plane, whatever their Burgers vector, direction line, the nature of the faults or the material, both for isotropic and for anisotropic elasticity.

The above relation was calculated for infinite dislocations. However, the influence of the bordering partial is not negligible when the size of the whole configuration is small. Gallagher (1966) has shown that the equilibrium value of d_e/d_i, which depends also on the forces arising from the end partials of the fault pair, is valid for segments of dissociated dislocations as long as the length of the segment is larger than $3d_i$. The widths of the two faulted ribbons were measured for different line

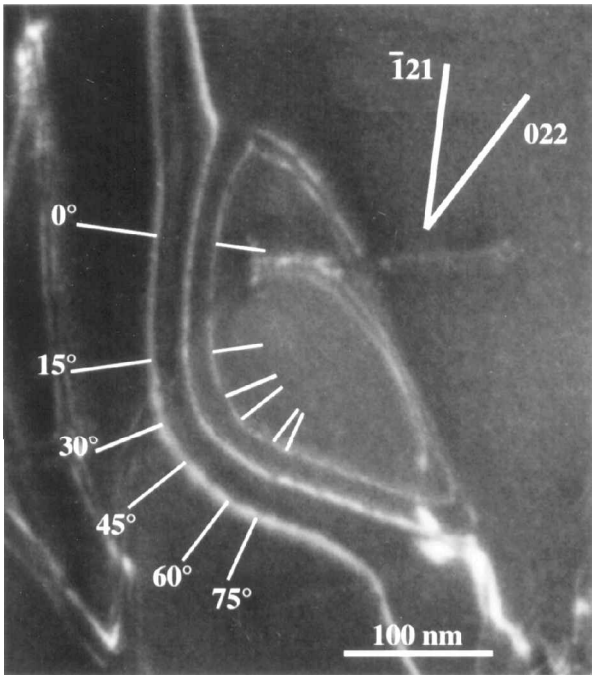

Figure 5. Example of the threefold configuration used to determine the d_e/d_i ratio ($\mathbf{g} = 0\bar{2}\bar{2}$; $\mathbf{B} = [\bar{1}\bar{1}1]$). The two faults are out of contrast. The positions of the measurements corresponding to different dislocation characters are indicated.

orientations of the Shockley partials in other configurations with a large extent. An example of such a configuration is given in figure 5. The different measurements lead to a value of $d_e/d_i = 0.74 \pm 0.1$ (figure 6) and putting this value into equation (12) yields

$$\frac{\gamma_i}{\gamma_e} = 0.82 \pm 0.08. \tag{13}$$

In order to estimate the actual values of γ_i and γ_e, numerical computations are necessary. We have assumed that the elastic constants of our alloy are not significantly different from the elastic constants of Ni_3Ge calculated by Yasuda *et al.* (1992) ($c_{11} = 263$ GPa, $c_{12} = 143$ GPa and $c_{44} = 103$ GPa). By computing the forces acting on the different partial dislocations within the framework of anisotropic elasticity, one finds that

$$\begin{aligned} \gamma_e &= 97 \pm 20 \text{ mJ m}^{-2}, \\ \gamma_i &= 80 \pm 20 \text{ mJ m}^{-2}. \end{aligned} \tag{14}$$

The APB energy on $\{111\}$ planes was also estimated. A separation distance of the $\frac{1}{2}\langle 110\rangle$ superpartials of 6 ± 1 nm in the screw orientation leads to

$$\gamma_{\text{APB}\{111\}} = 130 \pm 20 \text{ mJ m}^{-2},$$

which is close to the value obtained by Fang *et al.* (1994).

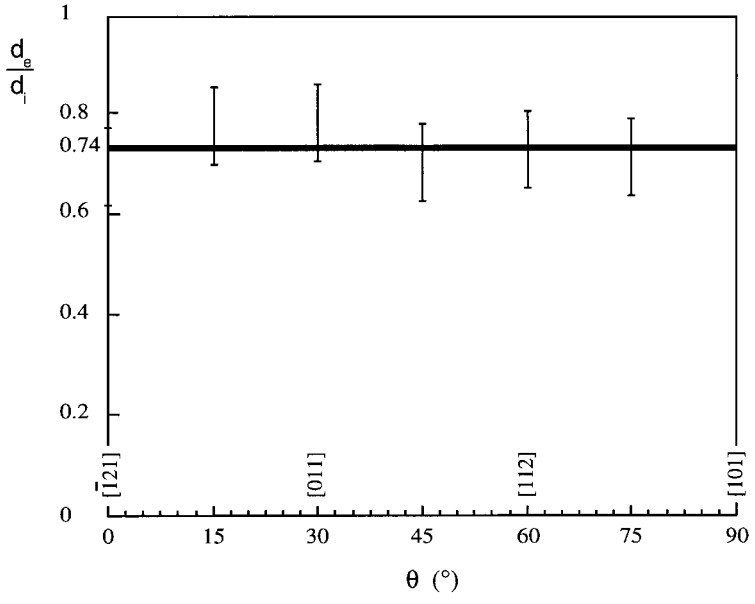

Figure 6. Experimental determination of d_e/d_i as a function of the character of the $\frac{1}{3}\langle 112\rangle$ partial dislocations. The mean value is close to 0.74.

4.2. *Relative stability of the threefold configuration*

Double-faulted ribbons configurations are observed. However, the relative stability of the threefold configuration (configuration 1)

$$\tfrac{1}{3}[\bar{1}21] + \text{SISF} + \tfrac{1}{3}[\bar{1}21] + \text{SESF} + \tfrac{1}{3}[\bar{1}21], \tag{15}$$

versus configuration 2

$$\tfrac{1}{2}[\bar{1}10] + \text{APB} + \tfrac{1}{2}[\bar{1}10] + \tfrac{1}{2}[011] + \text{APB} + \tfrac{1}{2}[011] \tag{16}$$

is questionable. Contrary to what happens for the undissociated configurations (reaction (5)), assuming the b^2 or Frank criterion, there is here no difference between the total self-energies of configurations 1 and 2 which can explain the transformation from configuration 2 to configuration 1. Moreover, in a first approximation the interacting $[\bar{1}10]$ and [011] superdislocations in the $[\bar{1}21]$ direction repel each other, thus preventing the interaction. The existence of the observed threefold configuration must then result from a gain in total energy, thus including the interaction energy and the fault energy which, in turn, depends on the orientation of the dislocations. The complete calculation of the energies of the configurations at equilibrium has been made using anisotropic elasticity. The energies of the two configurations are shown in figure 7 as a function of the character of the parent $\langle 112\rangle$ dislocation. The core energies are taken into account by changing the values of the cut-off radii used for self-energy calculations. As already pointed out (Saada and Douin 1991), the application of linear elasticity theory to the comparison of two different configurations necessitates some care, especially in the choice of the cut-off radii. Experimentally, configurations 1 can be observed with a screw or mixed character, but no configuration with a pure edge character has been found and, when the global line orientation changes towards the edge character, the threefold

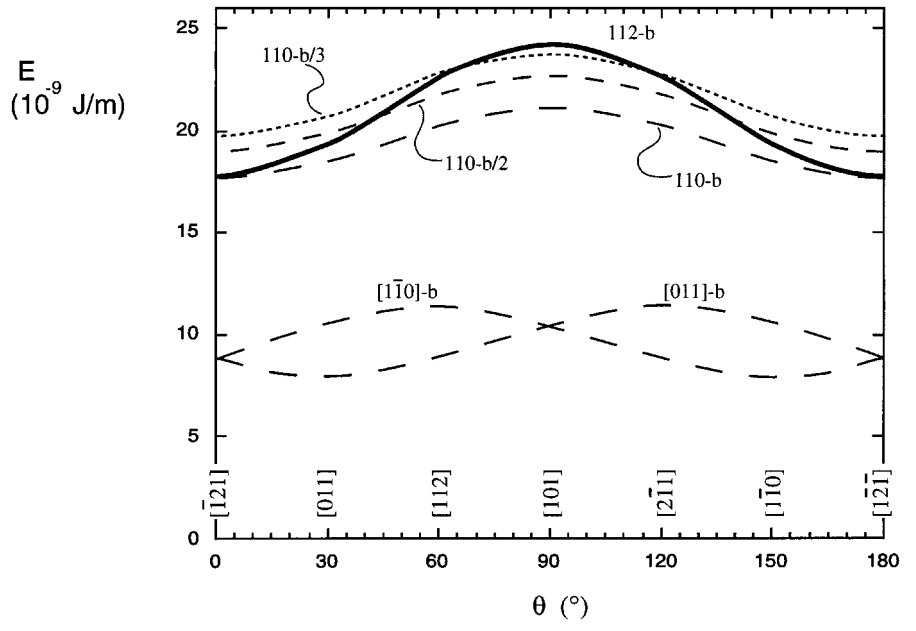

Figure 7. Energies of different configurations as functions of the line orientation and the core radius of the dislocations. 112-b is the calculated energy of configuration 1 with a chosen core radius of the $\frac{1}{3}\langle 112\rangle$ dislocation equal to the modulus of the Burgers vector, $\mathbf{b} = (a/3)\langle 112\rangle$; the cell parameter a is taken to 0.359 nm. 110-b, 110-b/2 and 110-b/3 respectively are the energies of configuration 2 with a chosen core radius of the $\frac{1}{2}\langle 110\rangle$ partial dislocations equal to b, $b/2$ and $b/3$ respectively. $[1\bar{1}0]$-b and [011]-b indicate the energies of $\langle 110\rangle$ dislocations dissociated according to reaction (1) before interaction.

configuration transforms into configuration 2 (see, for example, figure 5). This shows that configuration 1 has a lower energy than configuration 2 provided that the character of the dislocations is not too close to an edge type. Assuming a cut-off radius equal to the modulus of the Burgers vector for the $\frac{1}{3}\langle 112\rangle$ partial dislocations, the condition of the lower energy of configuration 1 versus that of configuration 2 for a character less than 75° can be attained only for a $\frac{1}{2}\langle 110\rangle$ cut-off radius smaller than or of the order of $b_{(1/2)\langle 110\rangle}/3$ (figure 7). The ratio of the cut-off radii must thus therefore satisfy

$$\frac{r_{c(1/3)\langle 112\rangle}}{r_{c(1/2)\langle 110\rangle}} \geqslant 3, \tag{17}$$

which indicates a larger relaxation of the core of the $\frac{1}{3}\langle 112\rangle$ partial dislocations relative to the $\frac{1}{2}\langle 110\rangle$ partial dislocations.

Finally, it must be pointed out that, even if dissociated $\langle 112\rangle$ dislocations have a slightly smaller line energy, the fact that they are observed with a rather small density indicates that they do not substantially multiply, a property which is believed to come from the low ability to move after formation. Note also that bordering $\frac{1}{3}\langle 112\rangle$ and $\frac{1}{6}\langle 112\rangle$ partial dislocations should also play a role in the extension of the threefold configuration as the exact processes of formation and destruction of

configuration 1 should depend on a zipping–unzipping type of process, which in turn is function of the mobility of the $\frac{1}{6}\langle 112\rangle$ and $\frac{1}{3}\langle 112\rangle$ bordering partials.

§ 5. Conclusions

Transmission electron microscopy investigations carried out on a $L1_2$ pseudo-binary Ni_3Ge-Fe_3Ge compound show the presence of a relatively high density of double-faulted ribbons of stacking faults in $\{111\}$ planes. They stem from the interaction of coplanar $\langle 110\rangle$ superdislocations, giving rise to a $\langle 112\rangle$ dislocation. It has been reported that the $\langle 112\rangle$ dislocations subsequently dissociate on to three identical Shockley partials with intrinsic and extrinsic faults in between. Energy calculations within the framework of anisotropy elasticity theory show that, provided that a larger core spreading of the $\frac{1}{6}\langle 112\rangle$ dislocations is assumed, the threefold dissociated configuration has a lower energy than the APB dissociated configuration.

References

Douin, J., 1991, *Phil. Mag. Lett.*, **63**, 109.

Douin, J., Kumar, K. S., and Veyssiere, P., 1995, *Mater. Sci. Engng*, **A192–A193**, 92.

Douin, J., Veyssiere, P., and Saada, G., 1998, *Phil. Mag.* A, **77**, 1323.

Edington, J. W., 1975, *Monographs in Practical Electron Microscopy in Materials Science*, Philips Technical Library, Vol. 3 (London: Macmillan), p. 17.

Fang, J., Schulson, E. M., and Baker, I., 1994, *Phils. Mag.* A, **70**, 1013.

François, A., Hug, G., and Veyssiere, P., 1992, *Phil. Mag.* A, **66**, 269.

Gallagher, P. C. J., 1966, *Phys. Stat. sol.*, **16**, 95.

Howe, L. M., Rainville, M. H., and Schulson, E. M., 1974, *J. nucl. Mater.*, **50**, 139.

Hug, G., 1988, PhD Thesis, University of Paris-Sud, France.

Hug, G., Loiseau, A., and Lasalmonie, A., 1986, *Phil. Mag.* A, **54**, 47.

Ivchenko, V.A., Syutkin, N.N., and Kuznetsova, T.V., 1986, *Phys. Metals. Metallorgr. (USSR)*, **64**. 146.

Kear, B. H., Oblak, J. M., and Giamei, A. F., 1970, *Metall. Trans.*, **1**, 2477.

Kear, B. H., and Wilsdorf, H. G. F., 1962, *Trans. metall. Soc. AIME*, **224**, 382.

Loretto, M. H., 1965, *Phil. Mag.*, **12**, 125.

Oblak, J. M., and Kear, B. H., 1971, *Electron Microscopy and Structure of Materials* (Berkeley, California: University of California), p. 566.

Saada, G., and Douin, J., 1991, *Phil. Mag. Lett.*, **64**, 67.

Suzuki, T., Oya, Y., and Wee, D.-M., 1980, *Acta metall.*, **28**, 301.

Takeuchi, S., and Kuramoto, E., 1973, *Acta metall.*, **27**, 193.

Tichy, G., Vitek, V., and Pope, D. P., 1986a, *Phil. Mag.* A, **53**, 467; 1986b, *ibid.*, **53**, 485.

Vanderschaeve, G., 1984, PhD Thesis, University of Lille, France.

Veyssière, P., and Douin, J., 1994, *Intermetallic compound*, vol. 1: *Principles*, edited by J. H. Westbrook and R. L. Fleisher, p. 519.

Yasuda, M. H., Tagasugi, T., and Koiwa, M., 1992, *Acta metall.*, **40**, 381.